# Polarity effects in unsupported polar nanoribbons

F. Güller,[1,2,3] A. M. Llois,[1,2,3,4] J. Goniakowski,[3,5,6] and C. Noguera[3,5,6]

[1]*Centro Atómico Constituyentes, GIyANN, CNEA, Avenida General Paz 1499, San Martín, Buenos Aires, Argentina*

[2]*Consejo Nacional de Investigaciones Científicas y Técnicas, Avenida Rivadavia 1917 (C1033AAJ), Buenos Aires, Argentina*

[3]*Laboratorio Internacional Franco-Argentino en Nanociencias (LIFAN)*

[4]*Departamento de Física Juan José Giambiagi, FCEyN-UBA, Intendente Güiraldes 2160 (C1428EGA), Buenos Aires, Argentina*

[5]*CNRS, Institut des Nanosciences de Paris, UMR 7588, 4 place Jussieu, 75252 Paris cedex 05, France*

[6]*UPMC Université Paris 06, INSP, UMR 7588, 4 place Jussieu, 75252 Paris cedex 05, France*

(Received 11 March 2013; published 17 May 2013)

We analyze the characteristics of polarity in unsupported nanoribbons with zigzag edges, by a combination of analytic models, semiempirical Hartree-Fock simulations, and first-principles approach. We consider two materials with widely different ionic-covalent character, MgO and $MoS_2$, and two polarity healing mechanisms: the so-called electronic compensation in ribbons with pristine edges, and ionic compensation in ribbons with an adequately chosen density of missing edge ions. The general expression of compensating charges, the edge metallization and spin polarization in the electronic mechanism, and the efficiency of the ionic mechanism are similar to those known in thin films and at polar surfaces. Differences, however, exist and are related to the low dimensionality, the atomic structure, and the strong undercoordination of edge atoms in nanoribbons. Polarity signatures are specified and a discussion of the possible origins of metallic edge states in these low dimensional objects is provided.

DOI: 10.1103/PhysRevB.87.205423 PACS number(s): 61.46.−w, 73.22.−f, 73.90.+f, 77.22.Ej

## I. INTRODUCTION

Polar surfaces of compound materials have been the subject of intense research in the past because of their prominent interest, both from fundamental and applied points of view.[1,2] More recently, the field has evolved towards the nanoscale, largely stimulated by the growing demand of novel materials for applications in microelectronics and heterogeneous catalysis. This is particularly true for ultrathin films, made of only a few atomic layers stacked along a polar direction, which have been shown to display a variety of new characteristics.[3–5] There have also been some advances in the controlled fabrication of small polar objects, such as nanoribbons, nanoislands, and nanoclusters,[6–13] with the focus put on how to control their growth in view of novel applications in optoelectronics, sensors, transducers, catalysis, and biomedical sciences among others.

While polarity concepts in ultrathin films are now rather well established, the same is not true in nanoribbons and nanoislands.[14] It is only recently that *ab initio* simulations of nanoribbons with polar edges have been performed, evidencing electronic properties close to those met in polar films, such as metallicity and magnetism,[15–27] in as various compounds as MgO, ZnO, BeO, $V_2O_5$, or $MoS_2$. However, in most cases, rather than referring to polarity, authors have drawn conclusions and made comparisons with edge states in graphene ribbons, which merely result from undercoordination effects.[28,29]

Triggered by this increasingly active research area, we wish to precisely assess the signatures of polarity in unsupported nanoribbons. Beyond classical electrostatic arguments given in Ref. 30, and some *ab initio* results on supported MgO ribbons,[31] in the present work, we consider zigzag nanoribbons of two different materials displaying widely different ionocovalent character: MgO and $MoS_2$. MgO is prototypical of a strongly ionic oxide, with a large band gap, crystallizing in the rocksalt structure. When unsupported, MgO(111) monolayers were shown to adopt a flat nonpolar geometry, with cation and oxygen atoms arranged in a h-BN-like manner.[32] Out of such a monolayer, two types of ribbons may be cut: armchair ribbons whose edges on both sides contain an equal number of anions and cations and thus are not polar, and zigzag ribbons which display alternating rows of anions and cations. The latter possess an obvious polar character and are the only ones we will consider in the present work. Figure 1(a) shows top and side views of an MgO(111) zigzag nanoribbon. $MoS_2$ is a semiconductor belonging to the transition metal dichalcogenide family. It displays a stacking of 2H-type trilayers, held together mainly through weak van der Waals interactions. Each trilayer is composed of a plane of Mo sandwiched by two sulfur planes. The Mo atoms are in a trigonal prismatic coordination, and are strongly covalently bound to S atoms within the same trilayer. Figure 1(b) shows top and side views of a zigzag edge nanoribbon cut out of a $MoS_2$ 2H trilayer, with the same type of alternating anion and cation rows as in the MgO ribbon. $MoS_2$ has received special attention due to its uses in the petroleum industry as catalyst and lubricant,[33,34] and more recently due to its potential applications in microelectronics.[35]

In this paper, by using a combination of analytic, semiempirical, and *ab initio* methods, we analyze polarity characteristics in nanoribbons with zigzag edges. We consider two compensation mechanisms:[1,2] electronic in ribbons with stoichiometric edges, and ionic in ribbons with an adequately chosen density of missing edge ions, and we decipher some new concepts behind edge polarity, as compared to thin-film polarity. The outline of the paper is the following. Section II describes dimensionality and size effects based on analytic arguments of general validity, relevant to polar nanoribbons in the large width limit. In Sec. III, relying on *ab initio* DFT simulations, we compare electrostatic, electronic, and energetic properties of MgO and $MoS_2$ zigzag ribbons,

 

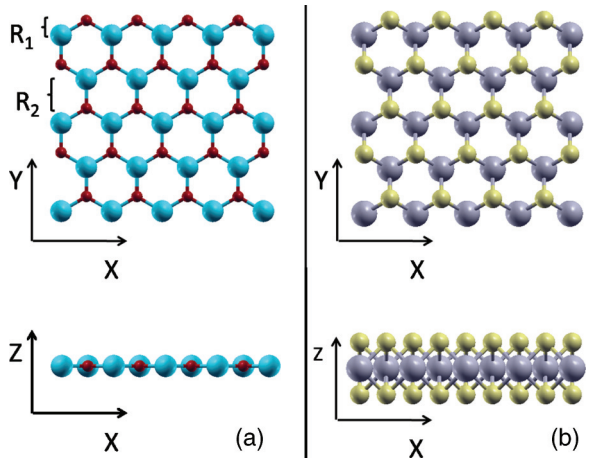


FIG. 1. (Color online) Zigzag ribbons, cut out of (a) a MgO(111) monolayer and (b) a $MoS_2$ 2H trilayer. Small spheres are O or S atoms. Big spheres are Mg or Mo atoms. The structures are periodic in the $X$ direction. The distances between successive atomic rows are denoted by $R_1$ and $R_2$.

with both stoichiometric and reconstructed edges. In the discussion, Sec. IV, we stress effects which result from the low dimensionality of these systems, in particular the asymptotic behavior of the electrostatic polar characteristics, we assess the signatures of polarity and we discuss the origin of edge states in polar nanoribbons. The understanding developed in this work is relevant for results obtained in the literature, in obviously polar nanoribbons, but in which polarity had not been recognized and should help placing them in the proper context.

## II. CHARACTERISTICS OF POLAR RIBBONS IN THE LARGE WIDTH LIMIT

In the earliest works on semi-infinite polar surfaces,[36–38] pure electrostatic considerations have proven to be an essential prerequisite for any understanding of their properties. Later on, the same was found for ultrathin films.[39] In this section, in order to derive the generic characteristics of polar ribbons in the large width limit, we start by recalling some purely electrostatic arguments.[30] Then we derive analytic models which account for two types of polarity compensation in unsupported ribbons, the so-called electronic and ionic mechanisms.[1,2]

### A. Macroscopic electrostatic model

In a first step, a macroscopic electrostatic approach, similar to the one used for surfaces[36–38] and thin films,[30] is used. The core idea is to model the ribbon as a series of alternating parallel wires with uniform linear charge densities $\pm\lambda$. Each wire represents a row of anions ($-\lambda$) or cations ($+\lambda$). Nearest-neighbor wires are separated by a distance $R_1$, and successive pairs by a distance $R_2$ (see Fig. 2). The ratio $\mathcal{R} = R_1/(R_1 + R_2)$ will quantify the strength of polarity effects. The ribbons are infinitely long and their width is measured by the number $N$ of pairs of rows.

The total electrostatic potential is the sum of all long-range contributions due to the charge densities per unit length $\pm\lambda$. The potential created by a single charged row at distance $d$ can

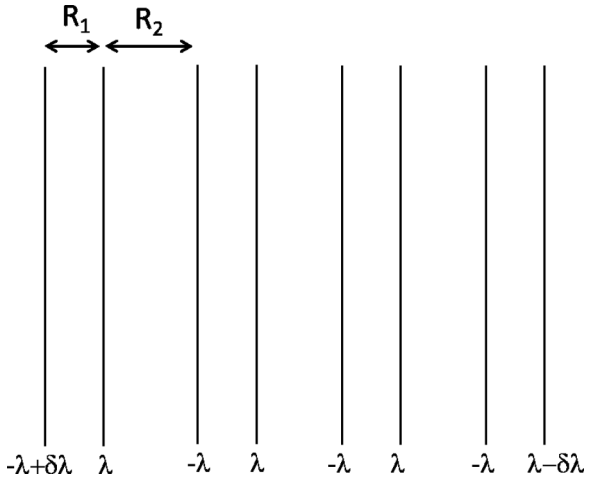


FIG. 2. Capacitor model for polar nanoribbons. Each row has a uniform charge density $\pm\lambda$. In the compensated regime, modifications $\delta\lambda$ appear on the outer rows.

be approximated by

$$V(d) \approx -2\lambda \ln d. \tag{1}$$

To avoid nonphysical divergence, a cutoff $b$ (of the order of an atomic distance) has to be introduced in the expression of $V(0)$, which yields $V(d = 0) = -2\lambda \ln 2b$.

The expressions for the total electrostatic potentials on the anion ($A$) and cation ($C$) rows, $V_{An}$ and $V_{Cn}$, are much more involved than for thin films, due to the logarithmic behavior of the Coulomb potential. Using the definition of the $\Gamma$ function[40] $\Gamma(n + \mathcal{R}) = (n - 1 + \mathcal{R})(n - 2 + \mathcal{R}) \ldots (1 + \mathcal{R})\Gamma(\mathcal{R} + 1)$, one finds that on the outermost cation row

$$V_{C1} = 2\lambda \ln \frac{(R_1 + R_2)\Gamma(N + \mathcal{R})}{2b\Gamma(N)\Gamma(\mathcal{R})} \tag{2}$$

while on the other side of the ribbon

$$V_{AN} = -2\lambda \ln \frac{(R_1 + R_2)\Gamma(N + \mathcal{R})}{2b\Gamma(N)\Gamma(\mathcal{R})}. \tag{3}$$

The potential difference $\Delta V = V_{C1} - V_{AN}$ across the ribbon reads

$$\Delta V = 4\lambda \ln \frac{(R_1 + R_2)\Gamma(N + \mathcal{R})}{2b\Gamma(N)\Gamma(\mathcal{R})}. \tag{4}$$

Its asymptotic expression, in the large $N$ limit, is obtained by using the Stirling formula $\Gamma(x) \approx e^{-x}x^{x-1/2}\sqrt{2\pi}$ for the $\Gamma$ function when its argument is large:

$$\Delta V \to 4\mathcal{R}\lambda \ln N, \tag{5}$$

which highlights the logarithmic divergence of this quantity in the large-$N$ limit.[30]

The total dipole moment per unit length is proportional to the ribbon width:

$$P = N\lambda R_1. \tag{6}$$

These size dependencies of $\Delta V$ and $P$ [Eqs. (5) and (6)], are characteristic of an uncompensated state.[41] The divergence of $\Delta V$ can be avoided by adding compensating charge densities $\pm\delta\lambda$ on the outer edges. This recipe is well known at surfaces and in thin films, and the stabilization of $\Delta V$ is referred to as

the healing of polarity. The new charge densities produce an additional electrostatic voltage, which, according to Eq. (1), reads

$$\Delta V_{\text{comp}} = -4\delta\lambda \ln[N(R_1 + R_2) - R_2], \tag{7}$$

as well as a contribution to the total dipole moment equal to

$$P_{\text{comp}} = -4\delta\lambda[N(R_1 + R_2) - R_2]. \tag{8}$$

The total potential difference and dipole moments are $\Delta V_{\text{tot}} = \Delta V + \Delta V_{\text{comp}}$ and $P_{\text{tot}} = P + P_{\text{comp}}$. Considering Eqs. (5) and (7), the cancellation of the divergence of $\Delta V_{\text{tot}}$ at $N \to \infty$ can be achieved by choosing

$$\delta\lambda = \mathcal{R}\lambda. \tag{9}$$

The same condition allows us to remove the linear dependence of the total dipole moment $P_{\text{tot}}$ as a function of $N$. Although $P$ and $\Delta V$ display different size dependencies than in thin films, this electrostatic criterion applied to charge densities per unit length is identical to that valid in thin films or at surfaces for charge densities per unit area.

To summarize, in the absence of polarity compensation, the voltage across the ribbon diverges as $\ln N$, and the dipole moment $P$ as $N$. Both divergences can be healed by the presence of compensating charges $\delta\lambda = \mathcal{R}\lambda$, the relationship between $\lambda$ and $\delta\lambda$ being formally similar to that valid for films. So far nothing has been said about the physical mechanism which produces these compensating charges. In the remainder of this section we consider an ionic-type mechanism and an electronic-type mechanism to account for the compensation of polarity.

### B. Size effects for ionic-type compensation

We now consider an ionic-type mechanism in which $\delta\lambda = \mathcal{R}\lambda$ is provided by adsorption of charged species (for example, edge hydroxylation) or by loss of ions (edge nonstoichiometry). The focus of this subsection is on the size dependence of the electrostatic properties of the ribbons in such compensated state, and more particularly on their asymptotic behavior.

In the presence of the compensating charge density $\delta\lambda = \mathcal{R}\lambda$ on the outer rows, the total voltage across the ribbon $\Delta V_{\text{tot}} = \Delta V + \Delta V_{\text{comp}}$ reads

$$\Delta V_{\text{tot}} = 4\lambda \ln \frac{(R_1 + R_2)\Gamma(N + \mathcal{R})}{2b\Gamma(N)\Gamma(\mathcal{R})} - 4\mathcal{R}\lambda \ln[N(R_1 + R_2) - R_2], \tag{10}$$

which, in the large-$N$ limit, scales as

$$\Delta V_{\text{tot}} = \Delta V_\infty + \frac{2\lambda\mathcal{R}}{N} \tag{11}$$

with $\Delta V_\infty = 4\lambda(1 - \mathcal{R}) \ln(R_1 + R_2) - 4\lambda \ln 2b\Gamma(\mathcal{R})$ in this model. In real systems, $\Delta V_\infty$ may involve some additional contributions, such as short-range electrostatic terms.

The total dipole moment $P_{\text{tot}} = P + P_{\text{comp}}$ no longer depends on ribbon width:

$$P_{\text{tot}} = N\lambda R_1 - \mathcal{R}\lambda[N(R_1 + R_2) - R_2] = R_2\mathcal{R}\lambda. \tag{12}$$

### C. Size effects for electronic-type compensation

Spontaneous modification of the electronic structure in response to the polar potential (edge metallization) provides another way of achieving charge compensation. It is the only compensation mechanism which can take place in unsupported ribbons with stoichiometric edges, in the absence of ion adsorption. The understanding of the compensating regime in that case is rather involved, since it requires taking into account the electronic structure explicitly. In this subsection, we develop an analytic model which goes beyond macroscopic electrostatics, in which short-range electrostatic interactions are taken into account, as well as electron transfers in a rigid-band approximation. This model is analogous to the one developed for ultrathin films in Ref. 39.

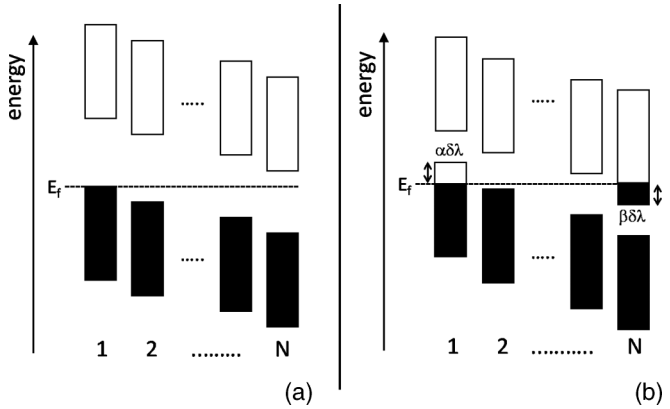


FIG. 3. Schematic electronic structure of polar nanoribbons in the (a) uncompensated and (b) compensated regimes.

Due to the variation of the electrostatic potential across the ribbon, as given by Eqs. (2) and (3), the energies of the local valence (VBs) and conduction bands (CBs) are shifted from their positions in the infinite layer. For narrow enough ribbons, they may not overlap and yield an insulating "uncompensated" electronic structure (Fig. 3 left panel). However, when $N$ becomes large enough, both valence states on one edge and conduction states on the other intersect the Fermi level, and a metallic band structure results, with modifications of the charge densities $\pm\delta\lambda$ on each edge due to changes in band filling (Fig. 3 right panel). This is the so-called electronic mechanism.

The long-range electrostatic potential which acts on the various layers includes two contributions: one due to the (unmodified) charge densities $\pm\lambda$, and the other due to the compensating charge densities $\pm\delta\lambda$, which in this model is assumed to be fully localized on the outermost rows on each side of the ribbon. Additionally, the $\pm\delta\lambda$ induce a correction, due to intra-atomic electron-electron interactions, on the outer layer potentials (with $U_A$ and $U_C$ the on-site Coulomb electron-electron interactions and $a$ the one-dimensional unit-cell parameter). The total electrostatic potential has also short-range contributions which differ in the central part and at the surface of the ribbon due to the different local environments. It may be accounted for by corrections $w_A$ and $w_C$ on the outer anion and cation layers, respectively, which do not depend on ribbon width (in the following, $\delta w = w_A - w_C$),

$$V_{C1} = 2\lambda \ln \frac{(R_1 + R_2)\Gamma(N + \mathcal{R})}{2b\Gamma(N)\Gamma(\mathcal{R})} + 2\delta\lambda \ln \frac{2b}{(R_1 + R_2)(N - 1 + \mathcal{R})} - aU_C\delta\lambda + w_C, \tag{13}$$

$$V_{AN} = -2\lambda \ln \frac{(R_1 + R_2)\Gamma(N + \mathcal{R})}{2b\Gamma(N)\Gamma(\mathcal{R})} - 2\delta\lambda \ln \frac{2b}{(R_1 + R_2)(N - 1 + \mathcal{R})} + aU_A\delta\lambda + w_A. \quad (14)$$

Assuming that the conduction-band minimum (CBM) and valence-band maximum (VBM) have major contributions from cation and anion orbitals, respectively,[42] in a rigid-band approximation, their energy positions become $\mathrm{CBM}_1 = \mathrm{CBM}^0 - V_{C1}$ and $\mathrm{VBM}_N = \mathrm{VBM}^0 - V_{AN}$, where $\mathrm{CMB}^0$ and $\mathrm{VBM}^0$ are the values in the absence of polarity. Assuming constant densities of states $1/\alpha$ and $1/\beta$ in the conduction and valence bands, respectively, the equalization of the Fermi level of both edges of the ribbon yields

$$E_F = \mathrm{CBM}_1 + \alpha\delta\lambda = \mathrm{VBM}_N - \beta\delta\lambda, \quad (15)$$

which allows us to write

$$\Delta V = G + \delta\lambda(\alpha + \beta), \quad (16)$$

where $G = \mathrm{CBM}^0 - \mathrm{VBM}^0$ is the band gap of the system in the absence of polarity.

The value of $\delta\lambda$ results, to order $1/N$:

$$\delta\lambda \approx \frac{4\mathcal{R}\lambda \ln N - \widetilde{G} - \delta w}{4 \ln N + \widetilde{V}} \quad (17)$$

with $\widetilde{V} = a(U_C + U_A) + \alpha + \beta + 4\ln(R_1 + R_2)/2b$ and $\widetilde{G} = G - 4\lambda \ln[R_1/2b\Gamma(\mathcal{R} + 1)]$. When $N$ goes to infinity, $\delta\lambda$ converges towards $\delta\lambda_\infty = \mathcal{R}\lambda = \lambda R_1/(R_1 + R_2)$ and the asymptotic limit is reached following a $1/\ln N$ law:

$$\delta\lambda \approx \delta\lambda_\infty - \frac{\widetilde{G} + \widetilde{V}\delta\lambda_\infty + \delta w}{4 \ln N}. \quad (18)$$

The voltage across the ribbon no longer diverges. It tends towards a constant value $\Delta V_\infty = G + (\alpha + \beta)\delta\lambda_\infty$, also following a $1/\ln N$ law.

The total dipole moment density $P = N\lambda R_1 - \delta\lambda(N(R_1 + R_2) - R_2)$ no longer diverges linearly with ribbon width as in the absence of compensating charges, but rather scales as $N/\ln N$:

$$P = \frac{N(R_1 + R_2)}{4 \ln N}(\widetilde{G} + \widetilde{V}\delta\lambda_\infty + \delta w). \quad (19)$$

The formation energy per unit length of the ribbon $E_{\mathrm{form}}$ can be calculated as the difference between the total energy per unit length $E_{\mathrm{ribbon}}$ and the energy of the corresponding number of formula units in the infinite monolayer $E_{ML}$:

$$E_{\mathrm{form}} = E_{\mathrm{ribbon}} - NE_{ML}. \quad (20)$$

Among the various contributions to $E_{\mathrm{form}}$, the electrostatic part is equal to $E^{el}_{\mathrm{form}} = 0.5\sum \lambda_i V_i$, where $\lambda_i$ and $V_i$ are the linear charge densities and potentials of each row, respectively. $E^{el}_{\mathrm{form}}$ has thus the same $N$ dependence as $\Delta V$ or $\delta\lambda$. In the large-$N$ limit, it diverges in the uncompensated regime ($\delta\lambda = 0$), while reaching a constant value with a $1/\ln N$ law in the compensated regime.

When $N \to \infty$, the band shift between two successive layers $\Delta V/N$ becomes negligibly small, which enables a "quasibulk" electronic structure being established in the central part of the film. In this limit, $\delta\lambda$ may be written

$$\delta\lambda = \delta\lambda_\infty - \frac{\Delta V_\infty \epsilon_\infty}{4 \ln N} + \cdots \quad (21)$$

with

$$\epsilon_\infty = \frac{\widetilde{G} + \widetilde{V}\delta\lambda_\infty + \delta w}{G + (\alpha + \beta)\delta\lambda_\infty}. \quad (22)$$

This expression is formally similar to the one derived for thin films.[39]

While the above derivation assumes that the film keeps a rigid structure, allowing for relaxation effects implies to replace the optical dielectric constant $\epsilon_\infty$ by the static dielectric constant (zero phonon energy) $\epsilon_0$, in Eq. (21). Therefore, all the aforementioned quantities ($\Delta V$, $\delta\lambda$ and $E^{el}_{\mathrm{form}}$) are expected to have the same $1/\ln N$ dependence both for the relaxed and rigid structures, but with a slope larger in the former case ($\epsilon_0 > \epsilon_\infty$).

To summarize, in this section, the generic width dependence of the electrostatic characteristics of polar nanoribbons has been derived in the large width limit. In the ionic compensation mechanism, compensating charges are provided by a well-defined density of missing ions on opposite edges and no strong modification of the electronic structure is necessary. The total dipole moment does not vary with $N$ and the asymptotic value of the voltage across the ribbon is reached in a $1/N$ manner. At variance, in the electronic mechanism, at work in polar nanoribbons with stoichiometric edges, compensating charges are provided by edge metallization and electron transfer between opposite edges. They hinder the formation energy and the voltage across the ribbon to diverge as the number of rows increases. Asymptotic values of $\Delta V$, $\delta\lambda$, and $E^{el}_{\mathrm{form}}$ are reached in a $1/\ln N$ way. A peculiarity is the size dependence of the total dipole moment which keeps diverging as $N/\ln N$. The value of the total dipole moment is thus not a good indicator of the state (compensated or not) of the system, at variance with polar surfaces or films.

## III. FIRST-PRINCIPLES RESULTS

This section is devoted to an accurate account of the energetics and electronic structure of MgO and $MoS_2$ nanoribbons in the medium size range. Considering these two largely different compounds allows us to check the importance of the gap width and the ionic/covalent ratio in the anion-cation bonding on the polar properties. We first present results of DFT electronic structure calculations of stoichiometric polar ribbons with zigzag edges and widths going from $N = 2$ to $N = 15$. Representative cases of reconstructed ribbons with missing edge atoms are then analyzed.

### A. Simulation setups

All calculations are performed using *ab initio* spin polarized density functional theory as implemented in the VASP[43] code. PAW pseudopotentials are used,[44] together with the generalized gradient approximation as parametrized by Perdew *et al.*[45] for the exchange and correlation potential. Self-consistent iterations are carried out until the difference in total energy between successive steps is smaller than $10^{-6}$ eV. The kinetic-

energy cutoff of the plane waves is set equal to 400 and 1000 eV for MgO and $MoS_2$,[46] respectively. The considered atomic valence electrons are $3s^2$ for Mg, $2s^2 2p^4$ for O, $3s^2 3p^4$ for S, and $4s^2 4p^6 4d^5 5s^1$ for Mo. All these structures are fully relaxed until residual forces drop below 0.01 eV/Å.

To model infinite one-dimensional (1D) ribbons periodic in the $X$ direction (Fig. 1) and avoid interactions between their periodic images, large cells of dimension 70 and 36 Å in the $Y$ and $Z$ directions are used for $MoS_2$ (respectively 60 and 30 Å for MgO), which leaves at least 30 Å vacuum in both directions, for all ribbon widths under consideration. The $k$-point grid in the corresponding first Brillouin zone is $9 \times 1 \times 1$ for MgO and $36 \times 1 \times 1$ for $MoS_2$. Charges are calculated according to the Bader's prescription.[47,48]

### B. $MoS_2$ and MgO ribbons with stoichiometric zigzag edges

#### 1. Ribbons of fixed width $N = 7$

We first consider MgO and $MoS_2$ ribbons of fixed width $N = 7$. Figure 4 shows the row-projected densities of states

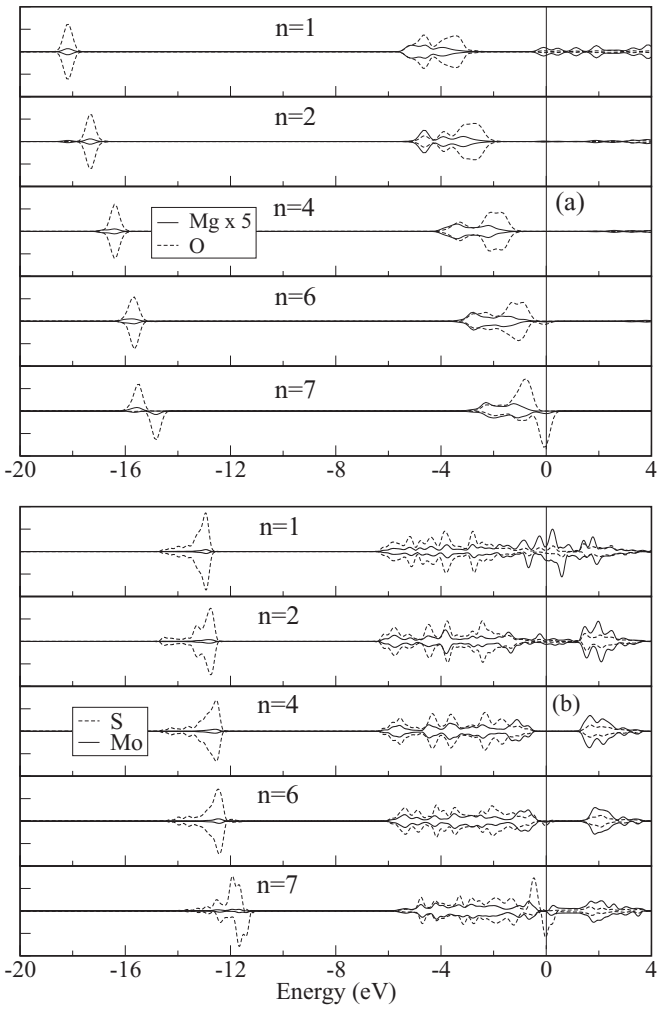


FIG. 4. Projected densities of states through (a) MgO and (b) $MoS_2$ relaxed zigzag nanoribbons with stoichiometric edges and $N = 7$ width. Row $n = 1$ is a cationic row. For simplicity, rows corresponding to $n = 3$ and $n = 5$ are skipped. The Fermi level is at zero energy.

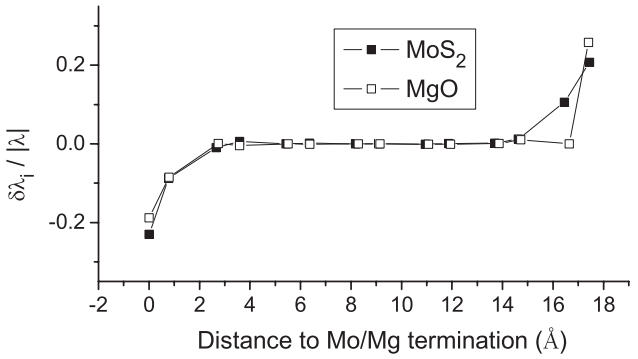


FIG. 5. Charge modifications $\delta\lambda_i/|\lambda|$, on each row $i$ through MgO and $MoS_2$ relaxed zigzag nanoribbons with stoichiometric edges and $N = 7$ width. Magnesium/molybdenum termination is on the left of the diagram.

(DOS) and Fig. 5 displays the modifications of Bader charges on each atomic row, relative to the ribbon center ($\delta\lambda_i/|\lambda|$). In the case of $MoS_2$, the charges of S atoms on both sides of the Mo plane are added.

The row-projected DOS evidence a progressive shift of the local VB and CB states, due to the electrostatic potential variations across the ribbon [Eqs. (13) and (14)]. This shift is more visible on the VB and even more on states with strong anion $s$ character (states below $-10$ eV). Both ribbons have a nonzero DOS at the Fermi level, due to an overlap of edge states. Such edge metallization is in agreement with the model developed in Sec. II C and with previous works.[15–20,24–27] These states receive contributions mainly from the $p$-type orbitals on the anion termination and the Mg $3s$ (Mo $4d$) orbitals on the opposite Mg (Mo) termination. It can be said that a *1D electron gas* is present on the ribbon edges. This metallicity, however, does not prejudge the existence of sizable conductivity on these edges. We will come back to the nature of edge states in the next section. Additionally, the ribbons display edge spin polarization.

The Bader charges on the outer rows differ from those on the ribbon center (Fig. 5). The modifications $\delta\lambda_i$ are located mainly on the two outermost rows on each side of the ribbons. In order to make a correspondence with the analytic model, a sum of the $\delta\lambda_i$ is performed separately on each side to obtain $\delta\lambda$. For both compounds, the resulting $\delta\lambda/\lambda$ values are close to the expected 1/3 value, as predicted by Eq. (9) for the zigzag ribbon geometry, where $R_2 = 2R_1$. The behavior of the electrostatic potential as well as the value of $\delta\lambda/\lambda$, are true signatures of polarity in these ribbons.

Differences between the two compounds involve the magnitude of the total band shift and the localization of the spin polarization. The band shift in the MgO ribbon is approximately 3 eV, more than two times larger than in $MoS_2$ (approximately 1.3 eV). This may be interpreted as due to the different values of the compensating charges $\delta\lambda_\infty = \mathcal{R}\lambda$ and of the gaps $G$, which enter the expression of $\Delta V$ in the model developed in Sec. II C ($\Delta V_\infty = G + (\alpha + \beta)\delta\lambda_\infty$). Indeed, the Mg charge $\lambda$ is ~30% larger than that of Mo, and the MgO monolayer gap (~2.8 eV) largely exceeds that of the $MoS_2$ trilayer (~1.6 eV), yielding a greater value of $\Delta V$. Additionally, short-range Coulomb interactions on the edges

$\delta w$ and bandwidth effects, $\alpha$ and $\beta$, could contribute but in a less obvious manner.

While all rows in the MgO ribbons display a well-defined separation between VB and CB, this is not the case in the $MoS_2$ ribbon. This difference may be assigned to the strength of undercoordination effects on the outer rows which turn out to be much stronger in $MoS_2$ than in MgO, and contribute to the metallization of the edges.

Spin-polarization effects are present in both compounds. They can be explained by high densities of states at the Fermi level, leading to an exchange splitting according to Stoner criterion. In relation to polarity, this argument has been used to explain the oxygen magnetic moment found at MgO(111) stoichiometric surface terminations by first-principles calculations.[49] It applies here too at the oxygen edges of MgO ribbons and at both Mo and S edges of $MoS_2$. At variance, the Mg edge is characterized by a more dispersive band and thus by a lower density of states, not allowing the Stoner criterion to be fulfilled. An estimate of the magnetic moments, obtained by integration of the spin polarized electron density in atomic spheres, is $0.38\mu_B$ per oxygen edge atom in MgO, $0.24\mu_B$ per edge atom at the S termination of $MoS_2$, and $0.57\mu_B$ at its Mo termination. A ferromagnetic spin ordering is found along the O edge in MgO, and Mo and S edges in $MoS_2$. No significant magnetic interaction exists between Mo and S edges in $MoS_2$ ribbons, in the limit of precision of the calculation. Similar spin ground states were found in simulations of other oxide[17,19,20] and $MoS_2$[22–24,27] zigzag nanoribbons.

### 2. Size effects

Beyond these results on ribbons of width $N = 7$, we have studied the size evolution of the formation energies $E_{\text{form}}$ and compensating charges $\delta\lambda/|\lambda|$ of MgO and $MoS_2$ zigzag ribbons (Figs. 6 and 7, respectively). $E_{\text{form}}$ is found to be an increasing function of $N$, but the maximum ribbon size, here ($N = 15$), does not allow it to actually enter the asymptotic regime. The formation energy is larger for $MoS_2$ than for MgO. However, their ratio is much smaller than the ratio of the bulk cohesive energies of the two compounds (approximately equal to 2). This points towards a lesser impact of polarity on $MoS_2$ ribbons than on MgO. A similar result had been obtained when comparing the impact of polarity on $SrTiO_3$ and MgO stoichiometric polar surfaces and assigned to a more efficient electrostatic screening of polarity in small gap compounds.[50]

Compensating charges are present for all widths and their value for large $N$ is close to 1/3. They are smaller for the MgO relaxed structures than for unrelaxed ones, in agreement with the discussion of dielectric constants in Sec. II C. According to Fig. 7, the asymptotic value of $\delta\lambda/|\lambda|$ is reached at larger sizes in MgO than in $MoS_2$. This result can be rationalized by comparing the slopes of the $1/\ln N$ terms in Eq. (21) for both compounds. The slope is equal to $\Delta V_\infty \epsilon_\infty = \widetilde{G} + \widetilde{V}\delta\lambda_\infty + \delta w$. As in the discussion of the voltage above, the larger slope in MgO can be mainly assigned to its larger gap and larger ionicity.

MgO ribbons of small widths ($N < 7$) undergo strong structural distortions. Their structure spontaneously transforms into a (001) ribbon with nonpolar [100] edges characterized by $\delta\lambda = 0$. This is in line with the structural transformations which take place in the small thickness regime in polar films, leading to nonpolar configurations.[32] On the other hand, $MoS_2$ zigzag ribbons are always stable, and strong relaxation effects

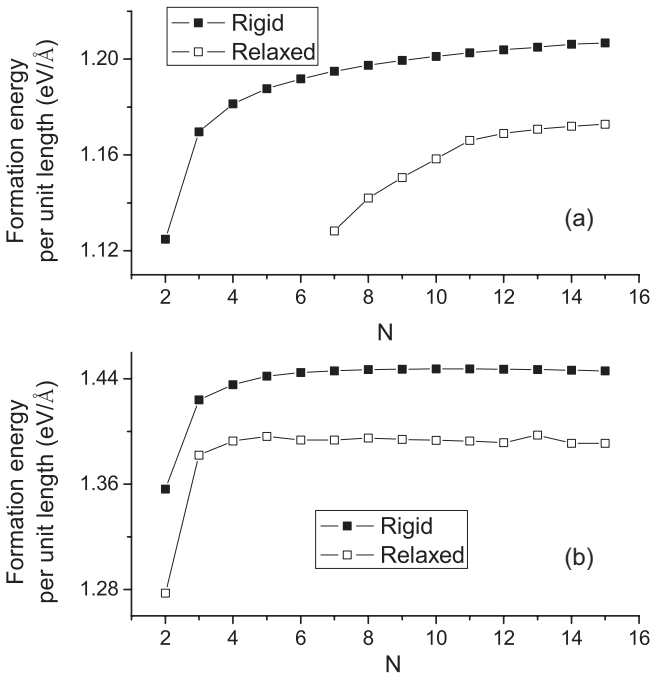


FIG. 6. Formation energy per unit length of (a) MgO and (b) $MoS_2$ zigzag nanoribbons with stoichiometric edges, as a function of width $N$.

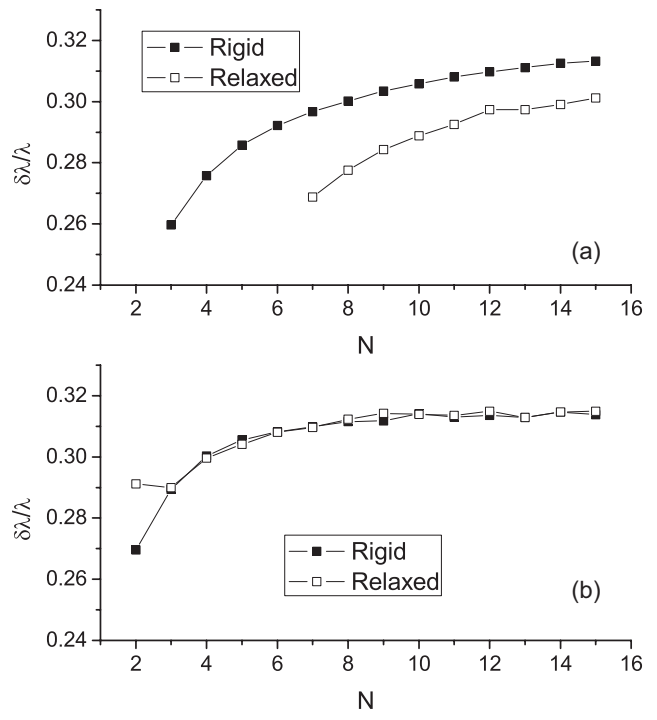


FIG. 7. Compensating charges $\delta\lambda/\lambda$ of (a) MgO (top) and (b) $MoS_2$ zigzag nanoribbons with stoichiometric edges, as a function of width $N$.

are observed only in the $N = 2$ case. Otherwise, relaxation effects are weak, much weaker in $MoS_2$ than in MgO, and mainly affect edge rows. No evidence of uncompensated polarity is found.

### C. Ionic compensation mechanism in reconstructed $MoS_2$ and MgO ribbons and comparison with the electronic compensation mechanism

In the previous section, we have analyzed the manifestations of the electronic compensation mechanism, which takes place in unsupported ribbons with stoichiometric edges ($\times 1$ unit cell). Here, we present the characteristics of $N = 7$ ribbons with reconstructed edges ($\times 3$ unit cell) with the goal to get insight into the ionic mechanism in $MoS_2$ and MgO ribbons and compare its characteristics to those of the electronic mechanism. For this purpose, we have removed one-third of the edge ions on both sides of the ribbons to fulfill the condition $\delta\lambda/ \mid \lambda \mid = 1/3$. In $MoS_2$ ribbons there are several ways of removing the two sulfur atoms per $\times 3$ unit cell. The one shown in Fig. 8 is found to be the most stable.

Figures 9 and 10 display the projected densities of states and charge distribution, respectively, for both compounds. Both quantities are averaged over the $\times 3$ unit cell and the structures are fully relaxed.

In both MgO and $MoS_2$ cases, the monotonic shifts of the local VB and CB states across the ribbons, observed in the stoichiometric zigzag ribbons (Fig. 4), are no longer present. In the MgO ribbon, the VB and CB states do not overlap and the electronic structure is semiconducting and nonmagnetic. In $MoS_2$, the band gap remains closed on the outer rows, as in the pristine zigzag structure, so that the reconstructed ribbon edges are metallic. Spin polarization is present only on the S termination, with ferromagnetic ordering, but the magnetic moment is localized mainly on the Mo atom on the underlying row, closest to both S vacancies ($\mu \sim 0.88\mu_B$). Interestingly, on this termination, the states at the Fermi level mainly come from Mo $d$ orbitals while S $p$ states are completely filled. In stoichiometric ribbons, the latter were partly depleted (Fig. 4).

In Fig. 10, the electron redistributions associated to both polarity compensation mechanisms are shown. They are found

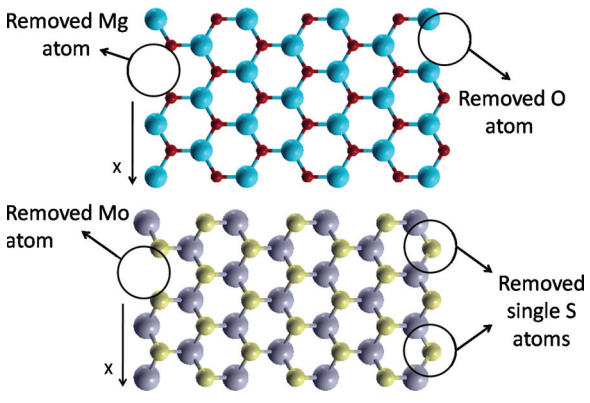


FIG. 8. (Color online) Reconstructed $N = 7$ MgO (top panel) and $MoS_2$ (bottom panel) unrelaxed ribbons, top view. Small and large spheres represent O/S and Mg/Mo atoms, respectively. The structure is periodic in the $X$ direction.

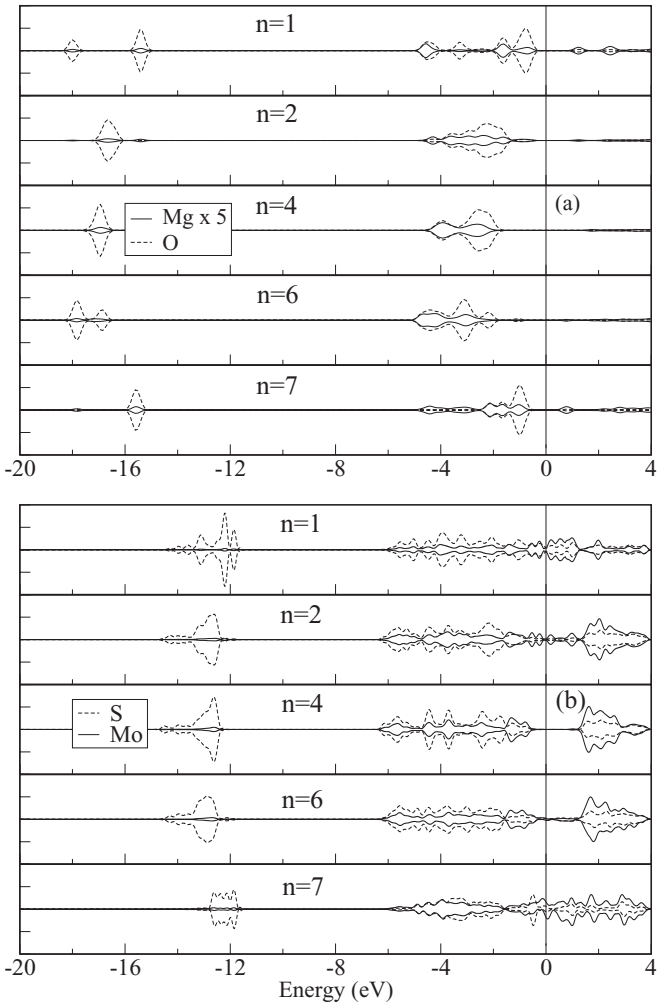


FIG. 9. Projected densities of states through (a) MgO and (b) $MoS_2$ reconstructed nanoribbons of $N = 7$ width ($\times 3$ unit cell average). Row $n = 1$ is a cationic row. For simplicity, rows corresponding to $N = 3$ and $N = 5$ are skipped. The Fermi level is at zero energy.

to be much smaller in reconstructed ribbons than in the pristine structures and display different behavior across the ribbons. In the pristine structure, the electron redistribution itself provides the compensating charges canceling the divergence of the voltage $\Delta V$ and the absolute value of $\delta\lambda$ is fixed by the electrostatic criterion. The values $\Lambda_n = \sum_{i=1}^{n} \delta\lambda_i / \mid \lambda \mid$ of the electron density variations integrated across the ribbons display a nearly constant value $\pm 1/3$ as a function of $n$ and only vanish when $n$ becomes equal to $N$ (integration over the whole width, fulfilling the neutrality condition. Such behavior is characteristics of an electronic dipole across the ribbon. At variance, in the ionic mechanism, the missing ions on the outer rows provide the compensating charges. The electron redistribution is a mere response to bond breaking at the edges and is thus much weaker than at pristine edges. The vanishing of $\Lambda_n$ somewhere inside the ribbons shows that the electron redistribution $\delta\lambda$ is equal to zero, at both edges. It is remarkable that the characteristics of the electron redistributions are very similar in MgO and $MoS_2$ ribbons, whatever the mechanism of compensation, despite their noticeably different edge

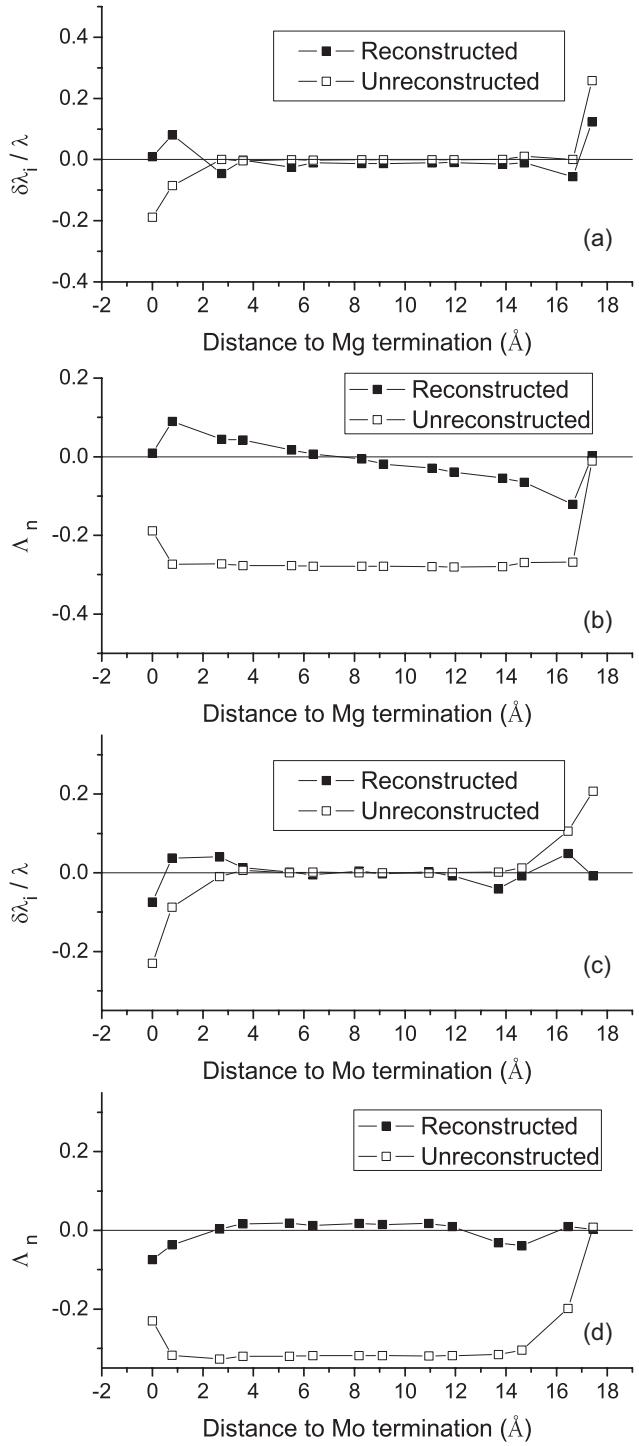


FIG. 10. From top to bottom: (a) Electron redistribution $\delta\lambda_i/|\lambda|$ and (b) integrated electron density values $\Lambda_n$ (see text) through unreconstructed and reconstructed MgO ribbons of $N = 7$ width; (c),(d) the same for $MoS_2$. In the reconstructed ribbons charges are averaged in the $\times 3$ unit cell and do not include the missing ion charges. Magnesium/molybdenum termination is on the left of the diagrams.

DOS characteristics when reconstructed (metallic in $MoS_2$, semiconducting in MgO).

$MoS_2$ reconstructed ribbons are thus characterized by an absence of band shifts, a filling of the S $p$ states on the sulfur termination (similar to that of oxygen $p$ states at the oxygen edge of MgO ribbons) and electronic redistribution characterized by $\delta\lambda = 0$. These features are characteristic of the ionic compensation mechanism for which the adequately chosen number of missing ions on the outer rows cancels the voltage divergence. The remaining metallicity can thus be assigned to undercoordination effects at edge atoms.

Reconstructed $\times 3$ ribbons turn out to be slightly more stable than their unreconstructed $\times 1$ counterparts. The energy differences per $\times 3$ unit cell are equal to 0.5 and 0.075 eV for MgO and $MoS_2$, respectively (0.05 and 0.008 eV/Å, respectively). This increased stability shows that the bond breaking necessary to obtain reconstructed edges costs less energy than the electronic compensation, even in the case of a small gap compound like $MoS_2$. This result is in line with the general findings on polar surfaces[1,2] although the numbers are quite small. The energy difference is much lower in $MoS_2$ than in MgO, which can be rationalized by remembering that the unreconstructed $MoS_2$ ribbons are proportionally more stable than the MgO ones (Sec. III B2). The energy difference values quoted above represent a lower bound to the efficiency of the ionic mechanism, since it is possible that more stable reconstructed configurations with larger unit cells exist. However, a systematic analysis of edge reconstruction effects is beyond the scope of this paper, whose aim was rather to identify polarity signatures in polar nanoribbons.

To summarize, all the unsupported zigzag nanoribbons analyzed in this work show signatures of polarity, similar to those observed in thin films,[2] and in agreement with the models developed in Sec. II. Characteristics of the ribbons are sensitive to undercoordination effects, which are strong in these low dimensional systems. Differences between the MgO and $MoS_2$ ribbons are related to the ionicity of both compounds (the value of $\lambda$), the width of the band gaps, the screening properties, and the existence of stronger undercoordination effects in the $MoS_2$ case.

## IV. DISCUSSION

The numerical simulations of MgO and $MoS_2$ ribbons, as well as the analytical predictions made in Sec. II, allow us to highlight some important characteristics of polarity in nanoribbons, related to the dimensionality of the systems, the nature of the edge states, and the competition between different compensation mechanisms.

### A. Dimensionality effects and asymptotic behavior

While, on general grounds, the scenarios of polarity healing by the electronic or ionic mechanisms in nanoribbons bear some resemblance to those known at surfaces of macroscopic samples or thin films, the logarithmic dependence of the electrostatic potential [Eq. (1)] which comes from the dimensionality of the ribbons has some distinctive consequences.

One consequence concerns the asymptotic regime, which is reached rather slowly in nanoribbons, especially in unreconstructed ones, so that the first-principles simulations performed in Sec. III up to $N = 15$ have not allowed us to reveal it. To complement first-principles simulations and support analytical arguments, in Figs. 11(a)–11(f), the width variations of the

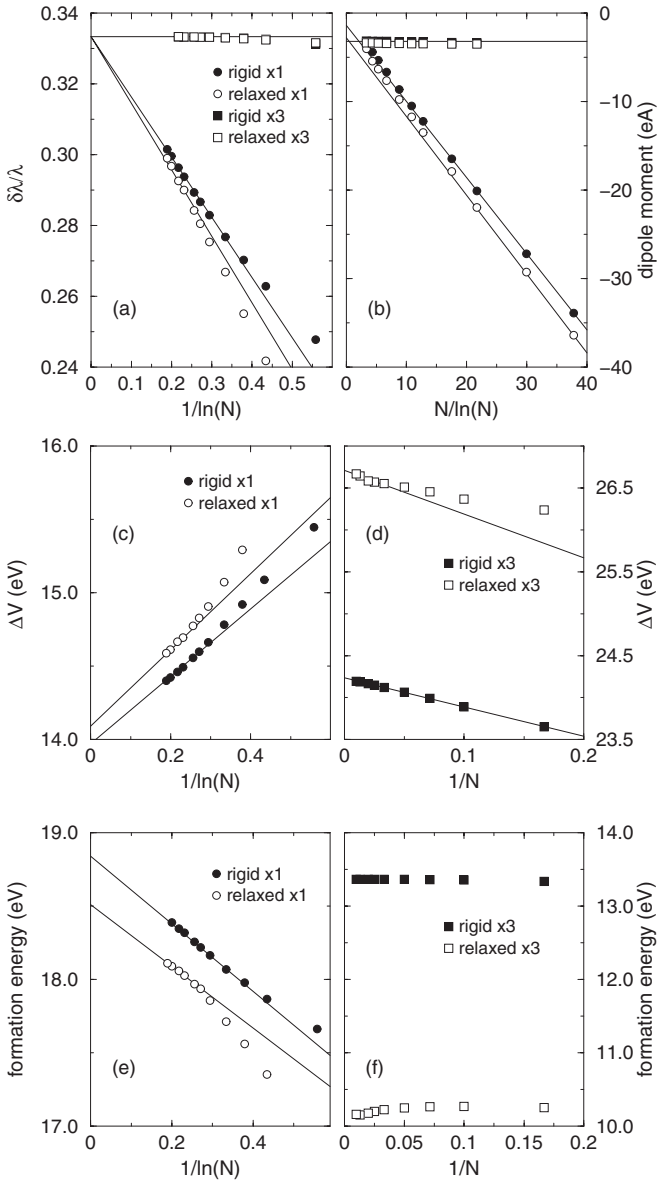


FIG. 11. Width variation of (a) the total compensating charges $\delta\lambda$, (b) the total dipole moment $P$, (c),(d) the voltage $\Delta V$, and (e),(f) the ribbon formation energy $E_{\text{form}}$ for unreconstructed ($\times 1$) and reconstructed ($\times 3$) ribbons. The straight lines show the asymptotic behavior of the various quantities.

compensating charges $\delta\lambda$, of the total dipole moment $P$, of the total voltage $\Delta V$, and of the ribbon formation energy $E_{\text{form}}$ are represented for unreconstructed and reconstructed MgO ribbons of width up to $N = 200$. They have been obtained by means of an order $N$ semiempirical Hartree-Fock code that we have developed,[51] with parameters necessary to simulate MgO systems determined in Ref. 51. In full agreement with the analysis made in Sec. II, in unreconstructed ribbons, $\delta\lambda/\lambda$ and $\Delta V$ reach their asymptotic values in a $1/\ln N$ manner. The $N \to \infty$ limit of $\delta\lambda/\lambda$ is $1/3$, as expected from the electrostatic criterion. The slope of these functions in the asymptotic limit, marked by the straight lines, is larger when relaxation effects are included, also in agreement with Eq. (21). The $N$ dependence of the ribbon formation energy $E_{\text{form}}$ is similar, showing that it is mainly driven by $\delta\lambda/\lambda$ and $\Delta V$. On the other hand, the dipole moment goes on increasing with $N$ despite the presence of compensating charges, but in a $N/\ln N$ manner, as predicted in Eq. (19).

At variance, in reconstructed ribbons ($\times 3$), aside from the small width regime where interactions between opposite edges (not taken into account in the analytic model) induce small size variations, the values of the total compensating charge (including the missing ions) and of the total dipole moment remain nearly constant as a function of $1/N$. The voltage displays linear variations as a function of $N$, as predicted by Eq. (11) while the formation energy does not display clear variations, being mostly constant. Relaxation effects are stronger in reconstructed than in $\times 1$ ribbons due to the increased number of undercoordinated atoms. Their effect on electrostatic properties goes beyond the mere use of a larger dielectric constant.

The nonlinear size scaling of the polar voltage in the ribbon uncompensated state [Eq. (5)] thus translates into specific electrostatic and electronic behaviors in the compensated states which differ from those present in thin films (Table I). When an ionic mechanism is at work, the leading term in $\Delta V$ varies as $1/N$ to be compared to a quasiconstant behavior in films. The size variations of the dipole moment, on the other hand, are similar for the two systems. At variance, when compensation is provided by an electronic mechanism and edge metallization takes place, the asymptotic values of $\delta\lambda$ and $\Delta V$ are reached in a $1/N$ fashion in films and, more slowly, in a $1/\ln N$ manner, in ribbons. The total ribbon dipole keeps increasing as $N/\ln N$ in the large width limit, which is not the case in thin films.

### B. Signatures of polarity and compensation

Aside from special cases of uncompensated polarity (see Sec. IV D), all polar systems in experiments or in numerical simulations are compensated. Recognizing polarity signatures is thus not always easy. Indeed, in a number of previous works, polarity had not been recognized as responsible for the properties of states near the Fermi level in zigzag ribbons with pristine edges, which were derived by a number of *ab initio* simulations. It is thus important to specify the actual signatures of polarity.

The first obvious signature of a polar stacking is the structure of the system itself. Using formal charges and knowing the prototypical spatial variation of the electrostatic potential for the dimensionality under consideration (films, ribbons, chains), it is easy to assess whether the stacking leads to a divergence of the voltage (Tasker's criterion for films[37]). In this respect, the zigzag ribbons of MgO, ZnO, BeO, $V_2O_5$, or $MoS_2$ considered in Refs. 15–27 were obviously polar, while the graphene ribbons to which some of these systems were compared are obviously nonpolar.

The present study brings a strong warning on the relevance of the dipole moment to inform about polarity.[30] For example, in compensated nanoribbons (electronic mechanism), $P$ goes on diverging at large size. This comes from the fact that, at variance with thin films, $P$ and $\Delta V$ are no longer proportional. In Ref. 30, we had provided two other examples of low dimensional systems (the one-dimensional chain of alternating anions and cations, and some symmet-

TABLE I. Behavior of compensating charges, voltage, and total dipole in polar thin films and nanoribbons.

| Compensation mechanism | Physical quantity | Thin films | Nanoribbons |
|---|---|---|---|
| Ionic | Voltage | $\Delta V - \Delta V_\infty = 0$ | $\Delta V - \Delta V_\infty \propto 1/N$ |
| Asymptotic behavior | Dipole moment | $P - P_\infty = 0$ | $P - P_\infty = 0$ |
| Electronic | Compensating charge | $\delta\sigma_\infty = R_1\sigma/(R_1 + R_2)$ | $\delta\lambda_\infty = R_1\lambda/(R_1 + R_2)$ |
| $N \to \infty$ values | Voltage | $\Delta V_\infty = G + (\alpha + \beta)\delta\sigma_\infty$ | $\Delta V_\infty = G + (\alpha + \beta)\delta\lambda_\infty$ |
| | Total dipole | $P_\infty = (G + \widetilde{V}\delta\sigma_\infty)/4\pi$ | $P_\infty \to \infty$ |
| Electronic | Compensating charge | $\delta\sigma - \delta\sigma_\infty \propto 1/N$ | $\delta\lambda - \delta\lambda_\infty \propto 1/\ln N$ |
| Asymptotic behavior | Voltage | $\Delta V - \Delta V_\infty \propto 1/N$ | $\Delta V - \Delta V_\infty \propto 1/\ln N$ |
| | Dipole moment | $P - P_\infty \propto 1/N$ | $P \propto N/\ln N$ |

ric nano-objects) similarly showing that the value of the dipole moment is not a faithful indicator of polarity. In one-dimensional chains, $P$ diverges with size, although no polarity is present. The situation is exactly opposite in some symmetric nano-objects, in which, although the total dipole moment is zero, polarity is present. The message is thus that although at semi-infinite surfaces and in asymmetric ultrathin films, it is legitimate to indifferently use the dipole moment value or the voltage to characterize polarity, since these two quantities are proportional, this is not a general property.

The actual indicators of compensated or uncompensated polarity are the voltage $\Delta V$ and the compensating charges $\pm\delta\lambda$. The electrostatic potential is the important quantity, since it determines a large part of the formation energies and electronic band characteristics. In uncompensated polar systems, it shifts the bands from one row to the other. When an ionic compensation mechanism is at work, the density of ions which has to be removed from the edges is determined from the condition that its associated potential cancels the total voltage divergence, leading to the condition $\delta\lambda/\lambda = \mathcal{R}$. Some electronic redistribution, in that case, takes place on the edges. It is characterized by $\delta\lambda/\lambda = 0$, as at nonpolar edges, and is irrelevant to polarity healing. In the electronic compensation mechanism, the row-projected DOS displays shifts across the ribbons which allow the overlap of VB and CB and charge modifications on the edges. The compensating electronic redistributions, as highlighted in Fig. 10, have to asymptotically obey the electrostatic criterion $\delta\lambda/\lambda = \mathcal{R}$ and induce a voltage across the ribbon.

### C. Physical origin of edge states

In polar systems, when a nonzero DOS is found at the Fermi level, the question may be asked whether this is due to undercoordination effects or to electronic compensation of polarity. This question is not only academic since conductivity properties may be very different in one case or the other. Indeed, the electronic mechanism of polarity compensation requires an overlap of edge bands. On the other hand, it is well known from many past surface science studies that undercoordination may induce one or the other of the following effects: presence of localized gap states (dangling bonds), surface metallization, opening or reduction of the gap compared to the bulk, depending upon the nature of the compound and the geometry of the surface. In graphene zigzag ribbons, for example, there are edge states built from unsaturated $sp^2$ orbitals (dangling bonds) due to atom undercoordination.

The comparison between MgO and $MoS_2$, in the present study, brings some insights into processes relevant for nanoribbons. In these systems, edge atoms are strongly undercoordinated: twofold to be compared to threefold for Mg, O, and S in the corresponding infinite layers, and fourfold to be compared to sixfold for Mo. In MgO, metallization occurs only when the edges are stoichiometric. When $\delta\lambda$ is provided by edge reconstruction (ionic mechanism), the electronic structure remains semiconducting with a mere gap narrowing.

At variance, in $MoS_2$ ribbons, metallicity takes place for both compensation mechanisms, but is associated to different underlying physical processes and different characteristics of the electron distribution. In reconstructed ribbons, there is no voltage across the ribbons which can induce an overlap of the VB and CB. Due to the more covalent character of the Mo-S bonding compared to Mg-O and the smaller gap, undercoordination effects are able to close the $MoS_2$ gap and lead to metallic edges. Regarding $MoS_2$ ribbons with pristine edges, it is likely that both undercoordination effects and electronic compensation are responsible for their edge metallic behavior. However, the latter drives the characteristics of the electron redistribution (value of $\delta\lambda/\lambda$ close to 1/3 and associated voltage), as in MgO.

### D. Other compensation mechanisms

In past studies, we had identified two mechanisms specific of the low thickness regime in ultrathin films, which are not at work at semi-infinite surfaces: a thorough structural transformation of the film[32] and the possibility of an uncompensated state.[41] We have found an equivalent structural transformation in the present study. For widths less that $N = 7$, MgO ribbons with stoichiometric edges spontaneously transform into (001) ribbons with nonpolar [100] edges. Both the local symmetry of the ribbons (from hexagonal to square) and the bulk structure from which the ribbons are cut (from h-BN to rocksalt structure) change.

As far as uncompensated polarity is concerned, the general argument that we had developed relied on the existence of a gap, the uncompensated state being stabilized as long as the voltage across the films is smaller than the gap [Fig. 3(a)]. Such a situation seems not to occur in MgO nor in $MoS_2$ ribbons. In MgO, narrow nanoribbons can relax towards the nonpolar (001) structural ground state, thus preventing an

uncompensated state to be stabilized. In $MoS_2$, additional effects could play a role, such as the presence of cation states at the top of the VB and/or the gap closure due to undercoordination at edge atoms, which were not considered in our description of the uncompensated polarity mechanism.[41] This is a delicate issue which is left for future works.

The goal of the present work was not to make a thorough study of all possible compensation mechanisms and their relative efficiency. We have only considered an electronic mechanism for the compensation of stoichiometric edges and, alternatively, a single reconstructed configuration providing the required compensating charges. In line with most results on polar oxide surfaces, we find that the latter yields lower formation energies for both compounds. However, the resulting stabilization is weak in the chosen systems. This may be due partly to the low ribbon dimensionality which allows smaller $\mathcal{R}$ values than at surfaces[31] and partly to the low electropositivity of Mo. Indeed, it has been found at some polar surfaces of transition metal oxides[2] that the electronic compensation mechanism is more efficient than the ionic one. There may also be ways to stabilize edge metallization purposely, for example by interaction with a metallic substrate[31] or by hydrogenation.[52] Here, behind the thorough analysis of polarity that we have performed, one of our goals was to place the results of numerous simulation works on ribbons with stoichiometric edges, in the proper context.

## V. CONCLUSION

In this paper we have analyzed the characteristics of polarity in unsupported nanoribbons with zigzag edges by relying on a combination of analytic models, semiempirical Hartree-Fock simulations, and first-principles calculations. As examples, we have considered two materials with widely different ionic-covalent character: MgO and $MoS_2$. We have studied two compensation mechanisms: electronic in ribbons with pristine edges, and ionic in ribbons with missing edge ions. We have been able to highlight resemblances and differences with polarity characteristics in thin films or at surfaces.

Resemblances include the asymptotic expression of compensating charges $\delta\lambda/\lambda = \mathcal{R}$, the edge metallization, accompanied by spin polarization, necessary to provide the compensating charges in the electronic mechanism, and the stabilization effect of the ionic mechanism compared to the electronic one.

Differences are related to low dimensionality, the atomic structure, and the strong undercoordination of edge atoms in nanoribbons. Dimensionality induces a nonlinear scaling of the polar characteristics. The Coulomb potential created by charged rows at a distance $d$ varies spatially as $\ln(d)$. This implies that the voltage across the ribbons and the total dipole moment are not proportional, the former being the important electrostatic quantity. Atoms at ribbon edges are usually more undercoordinated than at surfaces. Edge states resulting from this undercoordination may thus be present in the electronic spectra, with no relation to polarity.

Previous simulations of zigzag ribbons of various compounds had evidenced the presence of states at Fermi level, but most of them had failed to interpret them in terms of polarity. It is true that the roles of undercoordination and polarity cannot be easily separated by only looking at the total DOS. We have specified the actual polarity features for both compensation mechanisms. By comparing the electronic structures of ribbons with pristine and reconstructed edges in MgO and $MoS_2$ compounds, we have been able to assess that undercoordination does not induce the presence of edge states in MgO. In $MoS_2$ however, states at the Fermi level have a contribution from both polarity and undercoordination when the edges are stoichiometric (electronic mechanism) and only from the latter when ionic-type compensation takes place. We have highlighted differences in the electron redistribution induced by the two effects.

## ACKNOWLEDGMENTS

F.G. and A.M.L. belong to the Institute of Nanoscience and Nanotechnology (INN) of the Atomic Energy Agency (CNEA), Argentina. They acknowledge financial support from ANPCyT (Grants No. PICT-2011-1187 and No. PRH074) and CONICET (Grant No. PIP00273). We gratefully acknowledge a generous allocation of computing time at IDRIS, under Project No. 100170.

[1] C. Noguera, J. Phys.: Condens. Matter **12**, R367 (2000).
[2] J. Goniakowski, F. Finocchi, and C. Noguera, Rep. Prog. Phys. **71**, 016501 (2008).
[3] H-J. Freund, G. Pacchioni, Chem. Soc. Rev. **37**, 2224 (2008).
[4] N. Nilius, Surf. Sci. Rep. **64**, 595 (2009).
[5] F. P. Netzer, F. Allegretti, and S. Surnev, J. Vac. Sci. Technol. B **28**, 1 (2010).
[6] A. M. Ferrari, S. Casassa, C. Pisani, S. Altieri, A. Rota, and S. Valeri, Surf. Sci. **588**, 160 (2005).
[7] S. Agnoli, A. Barolo, G. Granozzi, A. M. Ferrari, and C. Pisani, J. Phys. Chem. C **111**, 19066 (2007).
[8] S. Benedetti, N. Nilius, P. Torelli, G. Renaud, H.-J. Freund, and S. Valeri, J. Phys. Chem. C **115**, 23043 (2011).
[9] Y. Pan, S. Benedetti, C. Noguera, L. Giordano, J. Goniakowski, and N. Nilius, J. Phys. Chem. C **116**, 11126 (2012).
[10] N. Nilius, S. Benedetti, Y. Pan, P. Myrach, C. Noguera, L. Giordano, and J. Goniakowski, Phys. Rev. B **86**, 205410 (2012).
[11] Q. Li, J. T. Newberg, E. Walter, J. Hemminger, and R. Penner, Nano Lett. **4**, 277 (2004).
[12] J. Zhang, J. M. Soon, K. P. Loh, J. Yin, J. Ding, M. B. Sullivian, and P. Wu, Nano Lett. **7**, 2370 (2007).
[13] C. L. Stender, E. C. Greyson, Y. Babayan, and T. W. Odom, Adv. Mater. **17**, 2837 (2005).
[14] C. Noguera and J. Goniakowski, Chem. Rev., doi: 10.1021/cr3003032.
[15] A. R. Botello-Mendez, M. T. Martinez-Martinez, F. Lopez-Urias, M. Terrones, and H. Terrones, Chem. Phys. Lett. **448**, 258 (2007).
[16] A. R. Botello-Mendez, F. Lopez-Urias, M. Terrones, and H. Terrones, Nano Lett. **8**, 1562 (2008).

[17]M. Topsakal, S. Cahangirov, E. Bekaroglu, and S. Ciraci, Phys. Rev. B **80**, 235119 (2009).
[18]Y. Wang, B. Wang, Q. Zhang, D. Shi, S. Yunoki, F. Kong, and N. Xu, Solid State Commun. **152**, 534 (2012).
[19]W. Wu, R. Lu, Z. Zhang, and W. Guo, ACS Appl. Mater. Interfaces **3**, 4787 (2011).
[20]Q. Tang, F. Li, Z. Zhou, and Z. Chen, J. Phys. Chem. C **115**, 11983 (2011).
[21]M. V. Bollinger, J. V. Lauritsen, K. W. Jacobsen, J. K. Nørskov, S. Helveg, and F. Besenbacher, Phys. Rev. Lett. **87**, 196803 (2001).
[22]H. Pan and Y. W. Zhang, J. Mater. Chem. **22**, 7280 (2012).
[23]C. Ataca, H. Sahin, E. Akturk, and S. Ciraci, J. Phys. Chem. C **115**, 3934 (2011).
[24]H. Pan and Y. W. Zhang, J. Phys. Chem. C **116**, 11752 (2012).
[25]R. Shidpour and M. Manteghian, Chem. Phys. **360**, 97 (2009).
[26]E. Erdogan, I. H. Popov, A. N. Enyashin, and G. Seifert, Eur. Phys. J. B **85**, 33 (2012).
[27]Y. Li, Z. Zhou, S. Zhang, and Z. Chen, J. Am. Chem. Soc. **130**, 16739 (2008).
[28]Sudipta Duttaa and Swapan K. Pati, J. Mater. Chem. **20**, 8207 (2010).
[29]Muge Acik and Yves J. Chabal, Jpn. J. Appl. Phys. **50**, 070101 (2011).
[30]J. Goniakowski and C. Noguera, Phys. Rev. B **83**, 115413 (2011).
[31]J. Goniakowski, L. Giordano, and C. Noguera, Phys. Rev. B **87**, 035405 (2013).
[32]J. Goniakowski, C. Noguera, and L. Giordano, Phys. Rev. Lett. **93**, 215702 (2004).
[33]T. A. Pecoraro and R. R. Chianelli, J. Catal. **67**, 430 (1981).
[34]P. D. Fleischauer, J. R. Lince, P. A. Bertrand, and R. Bauer, Langmuir **5**, 1009 (1989).
[35]B. Radisavlevic, A. Radenovic, J. Brivio, V. Giacometti, and A. Kis, Nat. Nanotechnol. **6**, 147 (2011).
[36]R. W. Nosker, P. Mark, and J. D. Levine, Surf. Sci. **19**, 291 (1970).
[37]P. W. Tasker, J. Phys. C **12**, 4977 (1979).
[38]R. M. Martin, Phys. Rev. B **6**, 4874 (1972).
[39]C. Noguera and J. Goniakowski, J. Phys.: Condens. Matter **20**, 264001 (2008).
[40]M. Abramowicz and I. A. Stegun, *Handbook of Mathematical Functions* (Dover, New York, 1970).
[41]J. Goniakowski, C. Noguera, and L. Giordano, Phys. Rev. Lett. **98**, 205701 (2007).
[42]In some compounds in which the top of valence band has a strong cation character, the voltage across the ribbon would rather be $\Delta V = V_{C1} - V_{CN}$, which would not qualitatively change the results of the model.
[43]G. Kresse and J. Hafner, Phys. Rev. B **47**, 558 (1993); G. Kresse and J. Furthmüller, *ibid.* **54**, 11169 (1996).
[44]P. E. Blöchl, Phys. Rev. B **50**, 17953 (1994); G. Kresse and D. Joubert, *ibid.* **59**, 1758 (1999).
[45]J. P. Perdew and Y. Wang, Phys. Rev. B **45**, 13244 (1992).
[46]Very high values of the plane-wave cutoff parameter are required in order to obtain accurate values of the compensating charges $\delta\lambda$.
[47]R. F. W. Bader, Chem. Rev. **91**, 983 (1991).
[48]G. Henkelman, A. Arnaldsson, and H. Jonsson, Comput. Mater. Sci. **36**, 354 (2006); W. Tang, E. Sanville, and G. Henkelman, J. Phys.: Condens. Matter **21**, 084204 (2009).
[49]J. Goniakowski and C. Noguera, Phys. Rev. B **60**, 16120 (1999).
[50]A. Pojani, F. Finocchi, and C. Noguera, Surf. Sci. **442**, 179 (1999).
[51]C. Noguera, J. Godet, and J. Goniakowski, Phys. Rev. B **81**, 155409 (2010).
[52]M. D'Angelo, R. Yukawa, K. Ozawa, S. Yamamoto, T. Hirahara, S. Hasegawa, M. G. Silly, F. Sirotti, and I. Matsuda, Phys. Rev. Lett. **108**, 116802 (2012).